

Global-local fatigue assessment of an ancient riveted metallic bridge based on submodelling of the critical detail

[Z. Liu](#)

[J. Correia](#)

[H. Carvalho](#)

[A. Mourão](#)

[A. de Jesus](#)

[R. Calçada](#)

[F. Berto](#)

Abstract

Increasing traffic demands (ie, load intensity and operational life) on ancient riveted metallic bridges and the fact that these bridges were not explicitly designed against fatigue make the fatigue performance assessment and fatigue life prediction of riveted bridges a concern. This paper proposes a global-local fatigue analysis method that integrates beam-to-solid submodeling, elastoplastic of material in local region, and local fatigue life prediction approach. The proposed beam-to-solid submodeling can recognize accuracy local stress/strain information accompanying with the global structural effect on the fatigue response of local riveted joints. The fatigue life is predicted based on cumulative damage rule, local strains, and number of cycles with consideration of traffic data, where the relation between the fatigue life and local strain is derived according to the Basquin and Manson-Coffin law. Besides, the elastoplastic of material is considered. The proposed methodology for fatigue life prediction based on local strain parameter and the Palmgren-Miner linear damage hypothesis is implemented in a case study of an ancient riveted bridge.

Nomenclature

- ***ADTT***
 - average daily truck traffic
- ***b***
 - fatigue strength exponent
- ***c***
 - fatigue ductility exponent
- ***D***
 - annual damage index
- ***E***
 - Young's modulus
- ***K'***
 - strain hardening coefficient
- ***N_f***
 - number of cycles to a initiate a macroscopic crack
- ***N_{f,i}***
 - number of cycles to failure under the stress range

- n_i
 - number of cycles under the particular stress range
- $\Delta\varepsilon$
 - total strain range
- $\Delta\sigma$
 - stress range
- $\Delta\sigma_i$
 - particular stress range ($i=, 2, \dots, k$)
- $\Delta\varepsilon_e$
 - elastic strain range
- $\Delta\varepsilon_p$
 - plastic strain range
- ε'_f
 - fatigue ductility coefficient
- σ'_f
 - fatigue strength coefficient
- ϕ
 - strain hardening exponent

1 INTRODUCTION

Fatigue is one of the main causes of in-service failures of steel structures under cycle traffic loading.^{1, 2} Significant fatigue damage can be taken even at low stress state under repeated stresses, leading to performance degradation and even costly repair.^{3, 4} In-service bridges, especially old riveted metallic bridges, are very susceptible to present high fatigue damage levels for variable traffic loads with increasing intensity, long operational period, and without anti-fatigue design originally. Fatigue-prone cracks have been detected in riveted bridges, as shown in Figure 1, which almost always initiate at the edge of the rivet hole in the outer ring of the rivet group.⁵ However, a number of riveted metallic bridges are still in operation, and many are expected to remain in service for the foreseeable future,^{6, 7} although many of those bridges have surpassed or are reaching the end of the original design life. Hence, accurate and efficient fatigue analysis method is consequently important to diagnose the current fatigue damage state and predict the remaining fatigue life of those structures, and suitable analysis models are then required for timely fatigue assessment and rehabilitation decision making of riveted bridges.

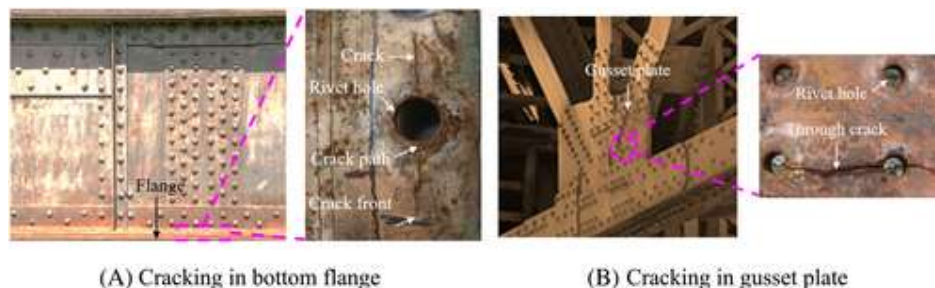


Figure 1
[Open in figure viewerPowerPoint](#)

Damage in the riveted joints [Colour figure can be viewed at wileyonlinelibrary.com]

Fatigue assessment based on the S-N approach requires the nominal stress evaluation on components under analysis, for comparison with the fatigue strength data. Since the riveted connections is an old fastening technique, a limited amount of S-N curves are available, and some design codes of current practice no longer refer explicitly the riveted joints (eg, EC3).^{8, 9} Additionally, applying code-based S-N curves, proposed for simple loading conditions, to real complex joints under complex loading reasonably is not well addressed. Local approaches to fatigue assessment have been proposed according to detailed stress/strain analyses,¹⁰ which can consider the elastoplastic due to stress concentration in the local structural discontinuity. Attempts have been made to better understand the fatigue performance of riveted joints in conjunction with local approaches.¹¹⁻¹³ Previous studies addressed the fatigue issues of riveted bridges mainly based on experiments of simple riveted joints or localized numerical simulation, which cannot fully consider the global effect of a structure on the fatigue response of various riveted joints for unrealistic boundary conditions. Additionally, few attempts were focused on the deterioration of material, which significantly affects the fatigue performance of riveted joints after service for long period.

Finite element (FE) simulation has been identified to be an effective way to capture the stress/strain state of structures.¹⁴⁻¹⁶ Fatigue FE analyses involving large-size structures usually demand huge calculations, especially when the plasticity of materials and the uncertainty of loading are considered.¹⁷⁻¹⁹ Basic models (ie, Beam or beam-link models) are inaccurate in fatigue analysis without including the detail geometry of components and the local plasticity of critical regions, whereas the refined model (ie, solid or shell model) of the whole structure usually consumes costly computational resources.²⁰ Hence, the global-local model that associates the global basic model and local refined model is desirable to achieve good balance between cost and efficiency in fatigue analysis.²¹ The global basic model is used to obtain global behaviors of the structure under loading and boundaries for the local refined model, and the local refined model can be utilized to capture localized information under the boundaries to account for global fatigue response. Integrated global beam model and submodel by using shell elements were applied to investigate the fatigue performance and of fatigue lives of rehabilitated riveted bridge joints of an ancient bridge based on code-based S-N curves.²² In this method, the submodel was built in the global model at concerned position rather than in a separated model, and the nonlinearity of material properties was not considered. This means that a single model needs to cover both the global model and multiple submodels when synchronous computation of multiple submodels is conducted,

which is time-consuming. Li et al²³ developed a global/local FE model coupling approach to assess the fatigue life of a countersunk riveted lap joint, which can take the nonlinearity of material properties, geometric deformation, and contact boundary conditions into consideration. In this approach, global model (shell elements) and local refined submodel (brick elements) were utilized together to achieve a good compromise between the simplicity and efficiency for components or structures. Whereas, it may not work in the large-span structures having a large number of components and joints, in which the global shell model of the large-span structures can take about huge computational cost.

To identify the local characteristics of fatigue damage in long-span structures accurately and efficiently, a methodology for global-local fatigue analysis considering the strain damage parameter applied in a local strain-life approach and the Palmgren-Miner rule is developed to explore the fatigue performance and predict the fatigue lives of riveted bridge joints in ancient metallic bridges, integrating global-local analysis based on beam-to-solid submodeling and elastoplastic of material in local region. This paper addresses the critical steps towards fatigue damage state assessment and fatigue life prediction of rivet joints; afterwards, case studies are conducted to validate the methodology with reference to an ancient riveted metallic bridge, and the fatigue life of riveted joints are evaluated.

2 GLOBAL-LOCAL ANALYSIS

2.1 Methodology

A systematic global-local analysis methodology for fatigue performance assessment and remaining life prediction of ancient riveted bridges is proposed, where beam-to-solid submodeling and the life prediction based on a local approach are integrated.

- Step 1

Material tests on the steel samples (ie, from replaced steels and new steels) are carried out to determine the material properties for the global model and submodel, such as Young's modulus and elastoplastic stress-strain curve.

- Step 2

The transient dynamic analyses are conducted in the global basic model to extract the dynamic boundaries for the local submodels of concerned joints under moving vehicle loads (eg, standard fatigue trucks specified in the design/evaluation codes, which are representative trucks with axle loads and wheelbases determined based

on equivalent fatigue with actual traffic loads), where the vehicle loads move forward after each load substep to simulate the movement of the vehicle.

- Step 3

Transient dynamic analyses are performed in the defined submodel to capture the stress state of local regions (ie, the ends of rivet holes).

- Step 4

The stress state around rivet holes is assessed for each component, and stress-time histories are processed to obtain stress amplitudes and corresponding number of cycles by a rain-flow counting method.

- Step 5

Fatigue life of the concerned joint is evaluated associated with a local approach based on strain criterion, which is derived from Basquin law, Manson-Coffin law, and the cumulative damage criteria.

Figure 2 shows the main steps for fatigue assessment by utilizing the proposed methodology. Essential background and details of key parts of the methodology are further addressed in the following sections of “*Beam-to-solid Sub-modeling Method,*” “*Rain-flow counting method,*” and “2.2 Fatigue life based on local approaches.” To effectively verify the proposed methodology, a case study was conducted.

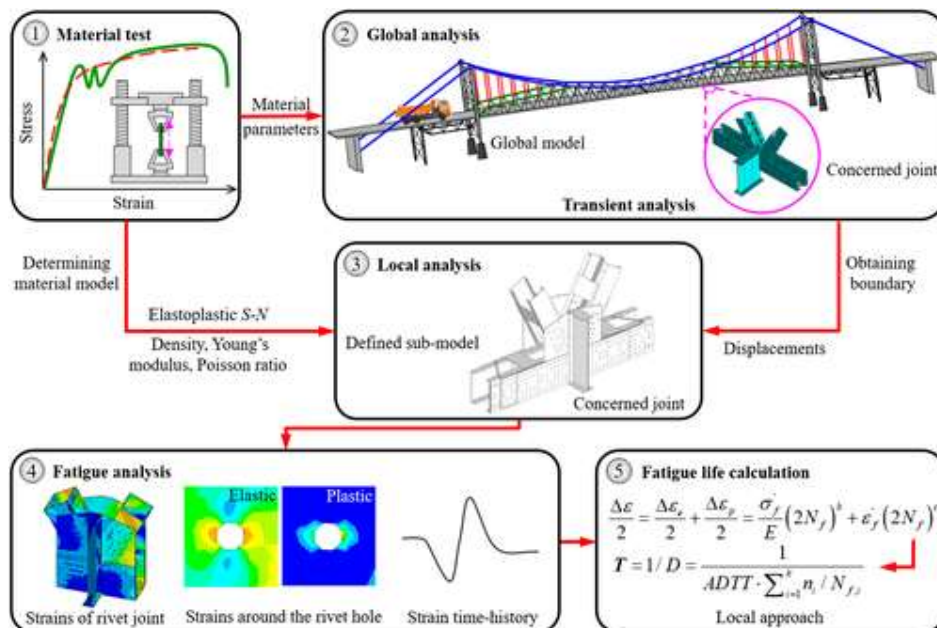


Figure 2
[Open in figure viewer](#)[PowerPoint](#)

Flow chart of the proposed global-local fatigue analysis [Colour figure can be viewed at wileyonlinelibrary.com]

2.1.1 Beam-to-solid submodeling method

Beam-to-solid submodeling method aims to obtain the boundary information (displacements and rotations or forces and moments) from beam elements and then transform to local refined solid model so as to capture detail localized information under efficient computation, as illustrated in Figure 3. The global FE model of the whole structures is created using beam elements and the local submodel of the concerned region is separately created using solid elements, where the FE software ANSYS 14.5²¹ can be used. In the submodel, pilot nodes are one-to-one created according to the boundary nodes of the global model and multi-point coupling (MPC) is defined between the pilot node and its corresponding slave node component so as to allow both displacement compatibility and stress equilibrium.²⁴ Hence, displacements and rotations of the boundary nodes of the concerned region in the global FE model are stored after global analysis and then assigned to the pilot node of the submodel. According to Saint-Venant's principle, the distribution of stress and strain is altered only near the regions of load application when an actual distribution of forces is replaced by a statically equivalent system. Besides, reasonably accurate results can be calculated in the submodel if boundaries of the submodel are far enough away from the stress concentration. Hence, special emphasis is focused on the length of submodel, where the length to height ratio of the boundary member in the submodel is recommended to be no less than four to ensure accuracy.^{25, 26}

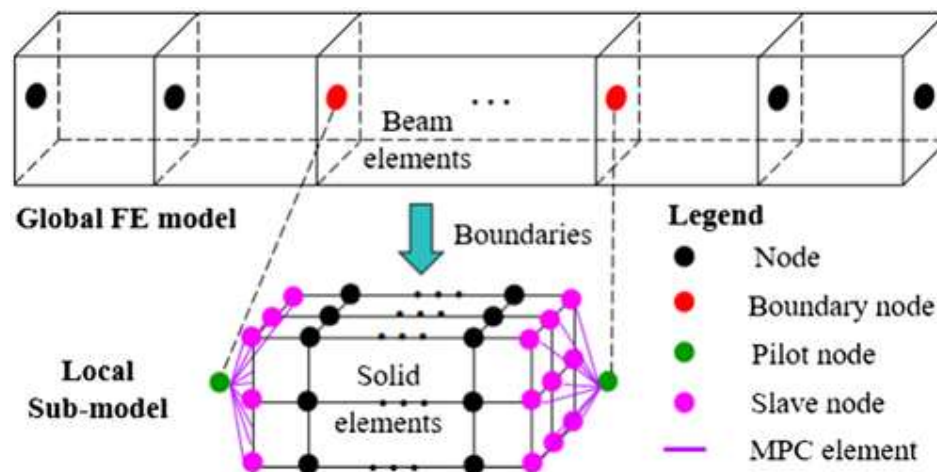
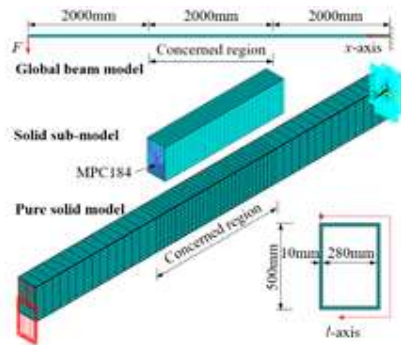


Figure 3

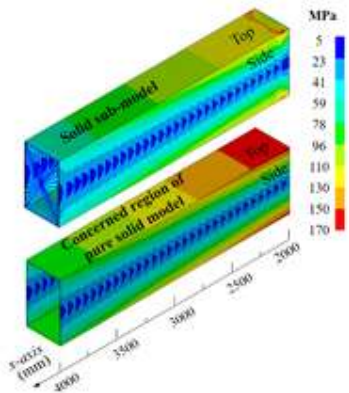
[Open in figure viewerPowerPoint](#)

Sketch of beam-to-solid submodeling [Colour figure can be viewed at wileyonlinelibrary.com]

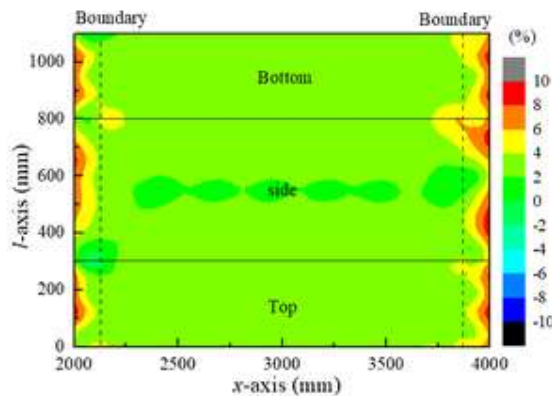
To demonstrate the accuracy of beam-to-solid submodeling, numerical tests were conducted based on a steel cantilever beam with a concentrated force (ie, $F = 90$ kN) acting at the end, as shown in Figure 4, whose cross section is rectangular tube with a thickness of 10 mm. A global beam model was built by using Beam188 elements according to the detail configuration presented in Figure 4A, and the middle 2-m-long concerned region was separately modeled by using Solid185 elements in FE software ANSYS 14.5.²¹ Besides, a pure solid FE model of the whole beam shown in Figure 4A was created by using Solid185 elements for comparison, where the element mesh of the concerned region was the same as that in the submodel. An isotropic linear elastic material was employed with Young's modulus equal to 2.05×10^5 MPa and Poisson's ratio equal to 0.3. Numerical simulations were conducted, and the results of the concerned region from the submodel and pure solid model were extracted for modeling verification, where the results from the pure solid model were used as the accurate results to calculate relative errors. Figure 4B shows the Von Mises stress contours of the concerned region of the solid model and pure solid model, where the stress distribution of the two model are similar except that stress disturbance exists around the ends of the solid submodel. The relative errors of the Von Mises stresses between the two models in Figure 4B are further calculated and illustrated in Figure 4C, where the local Cartesian l - x - z axes are built for expanded view and l is along the circumference of the cross section of the cantilever beam. It is observed that stresses of the solid submodel can match with those of the pure solid model with relative errors less than $\pm 10\%$ in most parts of the concerned region, such as the region from $x = 2250$ mm to $x = 2750$ mm, and with relative errors greater than $\pm 10\%$ just near the parts of boundary application. According to the Saint Venant's principle, the distribution of stress and strain is inaccurate only near the regions of load/boundary application when an actual distribution of forces is replaced by a statically equivalent system. Whereas, reasonably accurate results can be calculated in the submodel if boundaries of the submodel are far enough away from the stress concentration. Hence, the effectiveness of the beam-to-solid submodeling method can be identified with acceptable accuracy. Besides, since the boundaries of the solid submodel are extracted from the global beam model, the errors may mainly originate from the global beam model.



(A) Geometry model, beam-to-solid sub-model and pure solid model (Unit: mm)



(B) Von Mises stress contours of the concerned region in two models



(C) Relative errors of Von Mises stresses of the solid sub-model and pure solid model

Figure 4

[Open in figure viewerPowerPoint](#)

Numerical models and validation of beam-to-solid submodeling method [Colour figure can be viewed at wileyonlinelibrary.com]

2.1.2 Rain-flow counting method

Rain-flow counting method is one of four types of counting methods including in ASTM E1049-85²⁷ for fatigue analysis, which can convert a variable amplitude response time-history into a histogram of response ranges for cycles counting. Taking the variable amplitude stress time-history illustrated in Figure 5A as an example, the counting process is demonstrated in the following based on the method introduced in ASTM E1049-85.

- Step 1

Identify all of the relative peaks and valleys (ie, the dot points in Figure 5), denoting the absolute difference between any adjacent peak and valley as range.

- Step 2

Compare the current range with its previous range. If the current range is larger than its previous range, discard the first point in the previous range and moving the starting point to the second point in the previous range for the previous range containing the starting point of the stress history (as shown in Figure 5B,C,E) or count the previous range as one-cycle and discard the two points in the previous range (as shown in Figure 5D).

- Step 3

Read next range. If there are less than three point or out of data, execute Step 4 (as shown in Figure 5F); or repeat Step 2 (as shown in Figure 5E).

- Step 4

Count each range that has not been previously counted as one-half cycle.

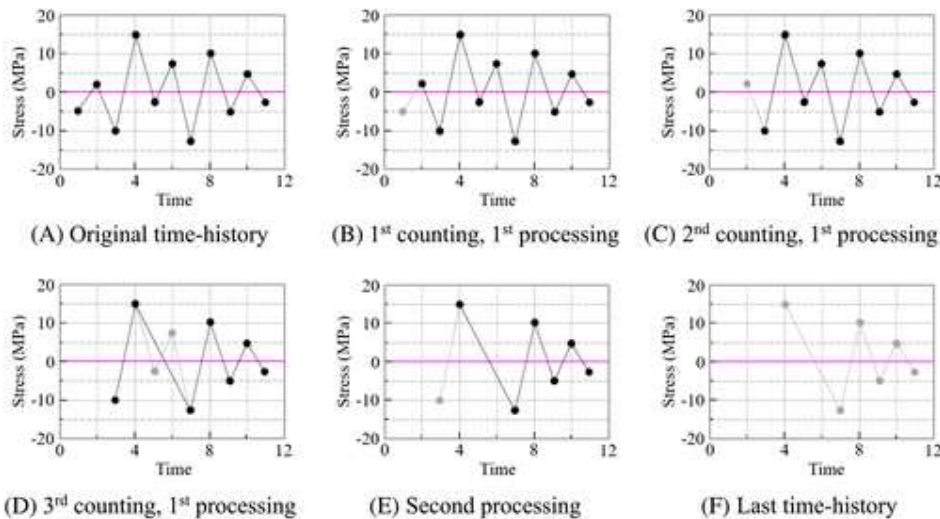


Figure 5

[Open in figure viewerPowerPoint](#)

Rain-flow counting example [Colour figure can be viewed at wileyonlinelibrary.com]

2.2 Fatigue life based on a local strain approach

In most practical cases, fatigue-induced cracks initiate around notches such as rivet holes in riveted joints for local stress concentration at the notch root, where plastic strains/stresses are imposed by surrounding elastic material.^{28, 29} The local approaches, recognizing the localized nature of the fatigue damage to assess the fatigue life, develop the correlation of the local response amplitude (eg, stress, strain) with endurance index to failure (eg, the number of cycles), where the elastic and plastic strain amplitude can be best described by the Basquin law³⁰ and the Manson-Coffin law.^{31, 32} Based on the proposal by Morrow,³³ the relation of the

total strain range ($\Delta\varepsilon$) and the fatigue life can be derived from superposition the elastic strain range ($\Delta\varepsilon_e$) and plastic strain range ($\Delta\varepsilon_p$), as presented in Equation 1.

$$\frac{\Delta\varepsilon}{2} = \frac{\Delta\varepsilon_e}{2} + \frac{\Delta\varepsilon_p}{2} = \frac{\sigma'_f}{E}(2N_f)^b + \varepsilon'_f(2N_f)^c \quad (1)$$

where N_f is the number of cycles to initiate a macroscopic crack; σ'_f and b are the fatigue strength coefficient and exponent; ε'_f and c are the fatigue ductility coefficient and exponent; $\Delta\sigma$ is the stress range; and E is the Young's modulus. The constant parameters in the equations can be determined from fatigue tests of smooth specimens under strain-controlled conditions.

The relation between the stress range and strain range can be usually expressed according to the Ramberg-Osgood equation, [34](#) as presented in Equation 2.

$$\frac{\Delta\varepsilon}{2} = \frac{\Delta\sigma}{2E} + \left(\frac{\Delta\sigma}{2K'}\right)^{1/\phi} \quad (2)$$

where K' and ϕ are the strain hardening coefficient and exponent. The cycle curve from the fatigue test can identify the constant parameters in Equation 2, which is the elastoplastic stress-strain relationship of the material and reveals the stabilized behavior of the material.

Combining Equations 1 and 2, the number of cycles to failure based on local approach can be determined when the stress amplitude is known, as given in Equation 3. Hence, the damage index caused by a stress amplitude can be expressed to be $1/N_f$.

$$\frac{\sigma'_f}{E}(2N_f)^b + \varepsilon'_f(2N_f)^c = \frac{\Delta\sigma}{2E} + \left(\frac{\Delta\sigma}{2K'}\right)^{1/\phi} \quad (3)$$

For stress time-histories with variable amplitudes due to actual traffic loads, the annual damage index (D) can be defined as Equation 4 based on Palmgren-Miner's rule. [35](#)

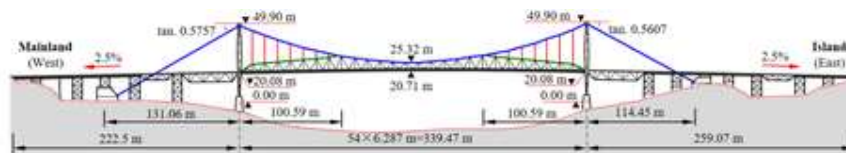
$$D = ADTT \cdot \sum_{i=1}^k \frac{n_i}{N_{f,i}} \quad (4)$$

where $ADTT$ is the average daily truck traffic, determined based on field traffic statistics; n_i and $N_{f,i}$ are the number of cycles under the particular stress range $\Delta\sigma_i$ ($i=, 2, \dots, k$) and the number of cycles to failure under the stress range; average daily truck traffic. Hence, the fatigue lives of fatigue-sensitive locations based on the fatigue truck specified in the design code can be expressed as $1/D$.

3 CASE STUDY: ANCIENT RIVETED METALLIC BRIDGE

3.1 Bridge description

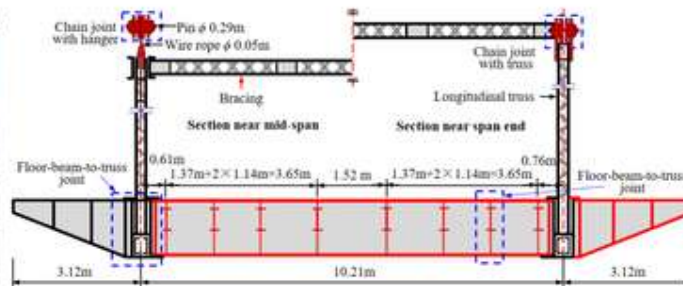
The Hercílio Luz Bridge (HLB), located between the Santa Catarina Island and the mainland of Brazil, is an eye-bar chain suspension bridge built in 1926, as shown in Figure 6A. The central span is composed of two longitudinal trusses, transverse floor-beams, longitudinal stringers, transverse bracings, and X-shape bracings, as shown in Figure 6B,C, whose central span is 339.47 m long and cross section is 16.45 m wide with two sidewalks.³⁶ At the 1/4 and 3/4 span point of the central span, the eye-bar suspension chains are integrated into the trusses, working as the upper chords of the truss; out the middle 1/2 span of the central span, the eye-bar suspension chains separate from the upper chords of the truss and link with it through vertical hangers. The bridge was designed by the same design company, using a similar concept as two American bridges, ie, the Silver Bridge and Saint Marys Bridge.³⁷ Four eye-bar in each suspension chain of the HLB instead of the two eye-bar specified for the other two bridge is the primary difference among them. The Silver Bridge collapsed on 15 December 1967 caused by the failure of a single eye-bar in the north chain near the west tower. After the collapse, the Saint Mary's Bridge was closed to traffic immediately and was then demolished for safety consideration. Nevertheless, the HLB was in service until 1982 and selected as a global heritage bridge for its historical significance and artistic monument in 1992.



(A) Configuration of the HLB



(B) Photograph



(C) Longitudinal truss

Figure 6

[Open in figure viewerPowerPoint](#)

Configuration of the HLB [Colour figure can be viewed at wileyonlinelibrary.com]

To maintain structural integrity and increase service life, a complete rehabilitation project was developed and currently underway for the bridge, including the replacement of compromised members (ie, sectional area loss due to corrosion more than 10%) and repair of the remaining members.³⁸ The rehabilitation complies with the provisions of the Brazilian codes and Eurocode, although the bridge was

originally completed according to the requirements of the American Association of State Highway and Transportation Officials at the time. According to the final rehabilitation design, the floor beam, stringer, eye-bar chain, and north sidewalk that are marked in red in Figure 6C are replaced by new members, and the remaining members are retained originally after repair or maintenance. In the rehabilitation, the new welded floor-beam is connected to the lower chord of the original built-up truss through rivets with a diameter of 22 mm in the rehabilitation; the new stringer (ie, welded I-beam) is connected to the web of the new floor-beam by welds and bolts, where the bolt connection is used to fix position in the welding process and strength the weld connection in the stringer-to-floor-beam joint. Relevant structural details of the floor-beam-to-truss joint and stinger-to-floor-beam are presented in Figure 7. The original longitudinal truss is made up of lower chords, uprights, diagonals, and upper chords, as shown Figure 8A, whose elements are riveted by steel plates, angels, channels, and lacings. The configurations of truss elements are illustrated in Figure 8B. As shown in Figure 8A, the floor-beam-to-truss joints and the truss-to-hanger joints are labeled as L0, L1, ..., L54 and U1, U2, U4, ...,U52, U53 from mainland to island, respectively. Besides, the hangers are labelled as H1, H2, ..., H7, H8, ..., H14.

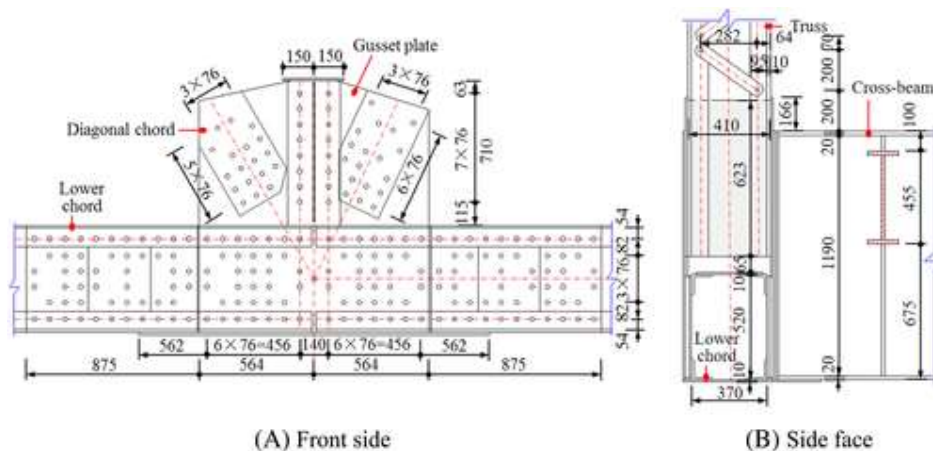
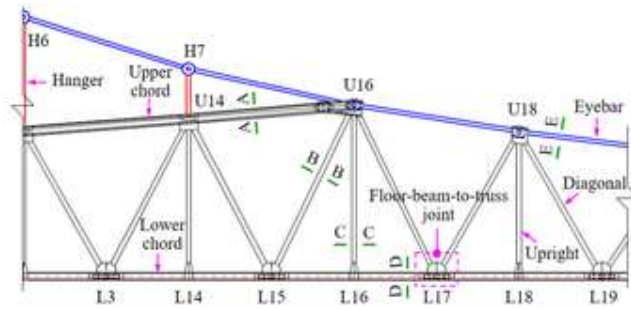


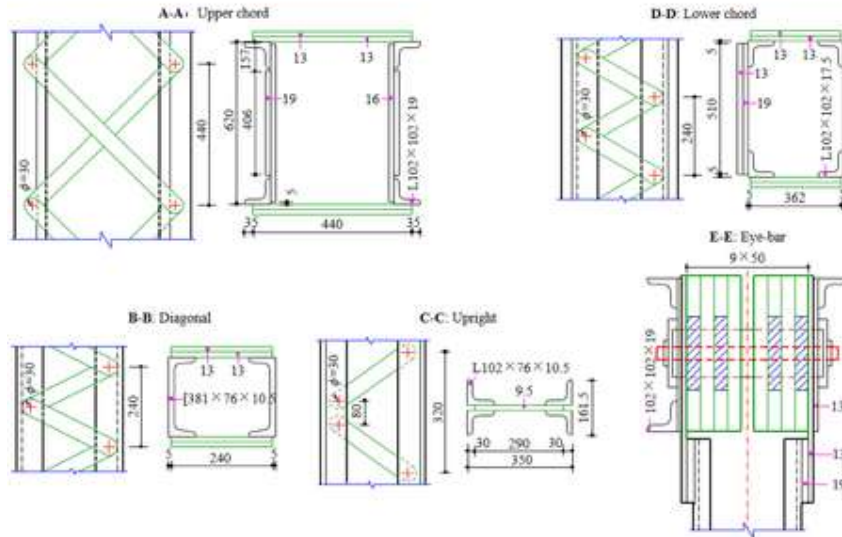
Figure 7

[Open in figure viewerPowerPoint](#)

Details of floor-beam-to-truss joint (unit: mm) [Colour figure can be viewed at wileyonlinelibrary.com]



(A) Truss



(B) Configurations of upper chord, diagonal, upright, lower chord and eye-bar (Unit: mm)

Figure 8

[Open in figure viewerPowerPoint](#)

Configurations of longitudinal truss and its elements [Colour figure can be viewed at wileyonlinelibrary.com]

3.2 Material characteristics

Mechanical properties of metal members on existing bridges are essential for the fatigue analysis, while the chemical and mechanical characteristics of the old steels in different bridges are fluctuant for no precise standardized material requirements and are not normally available in national standards. Besides, the mechanical properties of the components cycling used in the rehabilitation inevitably deteriorated within the original life of the structure, even though no severe damaged by corrosion initiated. Hence, tension tests have been conducted on standard test samples³⁹ in the laboratory of Federal University of Minas Gerais,⁴⁰ as shown in Figure 9A. The standard test samples were taken from the original structure of the HLB, where two were from the lower chord with the thickness of 12.00 and 11.97 mm, and the other ones were from the lower X-shape bracing with the thickness of 10.67 and 10.48 mm. According to the test data in Figure 9A, the average elastic modulus was

195.8 GPa, the average yield strength was 260.94 MPa, and the average tensile strength and average elongation at fracture were 437.35 MPa and 28.47%. Further, the primary chemical contents of the steel were examined, as presented in Figure 9B, evidencing a very low carbon content and confirming the ferritic structure.

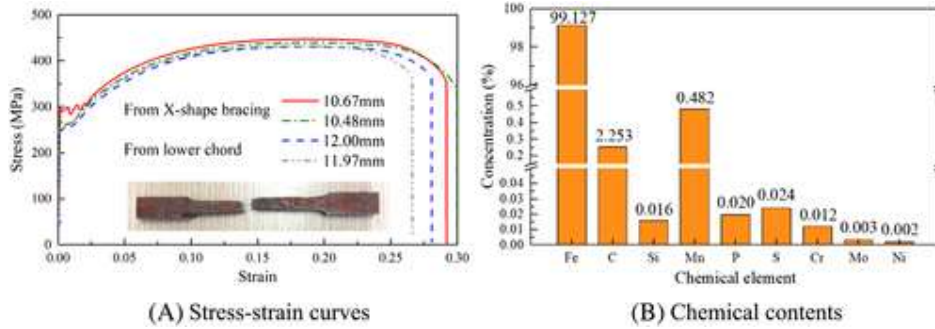


Figure 9
[Open in figure viewerPowerPoint](#)

Stress-strain curves and chemical contents of the original steel [Colour figure can be viewed at wileyonlinelibrary.com]

Based on the yield strength, tensile strength, and elongation at fracture of the tested material in Figure 9A, regression analysis of the Ramberg-Osgood equation was conducted to generate the elastoplastic stress-strain curve for the original member, as shown in Figure 11A. Hence, the parameters of the Ramberg-Osgood equation in Equation 2 can be determined, as shown in Figure 10A. Additionally, an elastoplastic stress-strain curve is adapted from de Jesus et al⁴¹ for the replaced member, as shown in Figure 10B. Besides, Figure 10 also presents the mechanical properties of the original and replaced member, including the density (ρ), Young's modulus (E), Poisson ratio (ν), and parameters for fatigue assessment.^{40, 41}

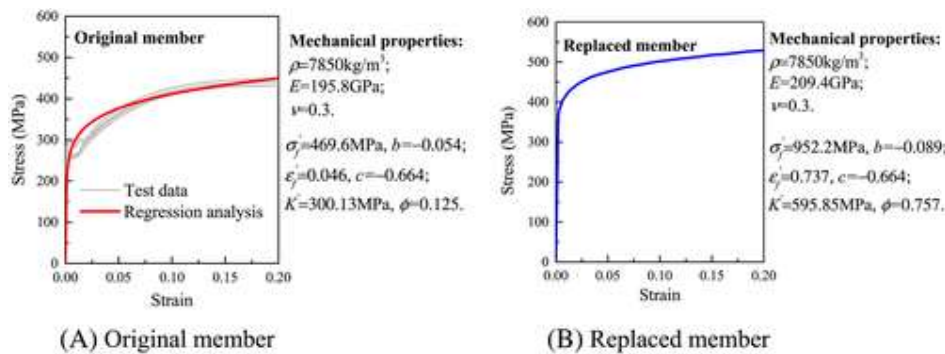


Figure 10
[Open in figure viewerPowerPoint](#)

Elastoplastic stress-strain curves and mechanical properties [Colour figure can be viewed at wileyonlinelibrary.com]

3.3 FE model

In order to obtain the global behavior and the boundary conditions of the submodel, a global FE model of the HLB was created within the FE software ANSYS 14.5,²⁴ as shown in Figure 11A, where the geometric constants (ie, areas of cross section, moments of inertia, etc.) were calculated according to the final design of rehabilitation. The elements used in the global FE model are listed in Table 1. Modeling details and model calibration of the global FE model can refer to the modeling process described in Liu et al.²² Boundary conditions of the global FE model were set as follows: the bottoms of the main towers and ends of eye-bar chains were fully restrained for all degrees of freedom (DOFs); the trusses were coupled with the columns of the main towers for all DOFs except for the rotational DOF around the z-axis at two ends. Linear elastic material properties, including the density, Young's modulus, and Poisson ratio, were assigned to the elements of original replaced components of the global model, which were separately presented in Figure 10A,B.

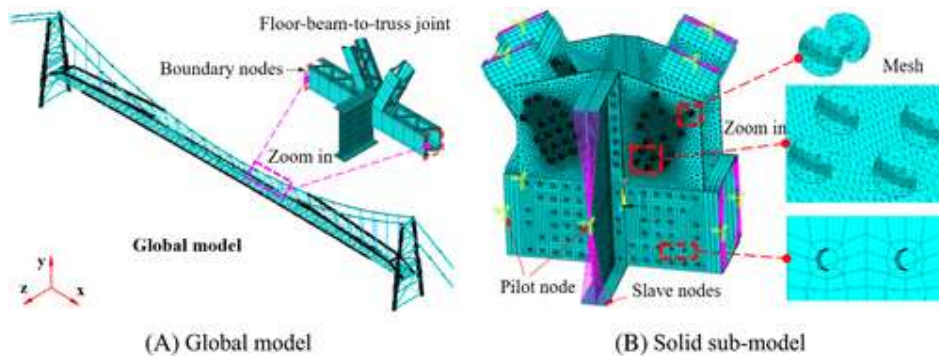
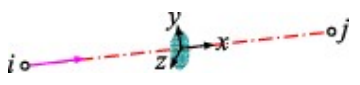





Figure 11

[Open in figure viewerPowerPoint](#)

FE model of the HLB [Colour figure can be viewed at wileyonlinelibrary.com]

Table 1. Element types used for global modeling

Component	Element Type	Illustration	Note
Eye-bar chain	Beam188		Released z-axis rotation DOF
Hanger	Link180		Tension only
Floor slab	Shell181		Four-node element

Component	Element Type	Illustration	Note
Truss, tower, girder	Beam188		With custom section

A refined 3D solid submodel of the concerned joint was created by using Solid185 elements, as shown in Figure [11B](#), which was independent of the global FE model. The submodel was generated by referring to the work in Hebdon et al [15](#) and Li et al [23](#) in which the load transfer between riveted plates was investigated. The submodel was created according to Figure [7](#), including plates, rivet holes, and rivets. Besides, target elements (TARGE170) and corresponding contact elements (CONTA174) were created to simulate the contacting surfaces between the rivet and surfaces of riveted plates, in which penetration of one surface over the other can be avoided. Friction force was specified between the contact surfaces, with the friction coefficient of 0.35 to simulate tangential behavior of contact surfaces. As rivet squeezing force strongly affects the stress distribution and fatigue fracture of plates around the rivet hole, [42](#) a fine mesh was conducted to the rivet and nearby region of riveted plates, while a coarse mesh was conducted for the regions of riveted plates away from the rivet hole. The elements have the sizes ranging from 8 mm around the rivet hold to 40 mm at the edge of the submodel. The complete rivets were created using a radially extruded shape and meshed with a global mesh size of 8 mm, as shown in Figure [11B](#). Those heads were hypothesized to be half-round with a diameter of 44 mm. By reducing the temperature of the rivet shank along the longitudinal rivet axis, squeezing force between riveted plates is generated, where an average squeezing force of about 82.7 MPa existed between rivets plates according to previous investigation. [43](#) An orthotropic thermal expansion coefficient of 1.2×10^{-5} ($1/^\circ\text{C}$) was defined for the rivet shank along its longitudinal axis. To obtain an approximately equal squeezing force level, a temperature of 55°C was applied to the nodes of the rivet shank in the initial step, and the temperature of these nodes was then reduced to 20°C (ie, the design temperature) to simulate the tension in the rivet shank. Since high redundancy exists in the lower chords fastened with many rivets, lower chords are usually not the most vulnerable part. In the chords, the rivets were not built, and the nodes around those rivet holes were merged, where the element sizes were 14 mm. Such a simulation method was implemented to consider the simplified squeezing effect in the regions of lower chords, and the number of elements and contact relationships were reduced.

Rigid MPC was defined between each pilot node and its corresponding slave node component through MPC184 elements. The submodel was assigned with the same density, Young's modulus, and Poisson ratio as the global model, as shown in Figure 10A. Besides, to simulate the plastic behavior, two elastoplastic stress-strain curves in Figure 10A,B, are, respectively, defined and assigned to corresponding elements of original and replaced members in the submodel.

3.4 Fatigue analysis

Load generated by vehicles is generally very complex for the variability of vehicle geometry and uncertainty of traffic.⁴⁴ Hence, typical fatigue load models have been defined in bridge design codes or specifications (ie, Eurocode⁴⁵ and Association of State Highway and Transportation Official code⁴⁶) to present the actual traffic load conditions accurately through equivalent fatigue damage at specific details for simplification and uniform standard. As the HLB located in Brazil, a three-axle fatigue truck model with a total weight of 300 kN, generating from actual Brazilian traffic load,⁴⁷ is adopted for fatigue analysis for better presenting the native traffic situations. The front axle is 60 kN, and the other two axles are both 170 kN. The wheelbases are 5.2 and 1.3 m from the front of the truck to the back, and wheel track is 1.9 m. The contact areas of tires are assumed to be a square with a length of 0.40 m.

The transient dynamic analyses are conducted in the global model under the moving fatigue truck specified in the specified in the design codes to obtain the boundaries of the concerned joints, where the wheel loads move forward after each time step to simulate the movement of the truck. The first time step is assigned with a very short duration of 0.001 second with the time integration shut down, where only self-weight of the bridge is applied so as to provide the initial state for the subsequent time steps. Thereafter, time steps are determined according to the speed of the truck, starting location (ie, the bridge end) and loading location with time integration started up, where the speed is defined as 22.03 m/s (ie, 79.3 km/h) according to the weigh in motion traffic measurements in Brazil.⁴⁷ The boundaries of the concerned joints in each time step are sorted in an external text file, and the stress time-histories of members in global can be obtained to preliminary analysis, such as determining the critical joints.

Thereafter, analysis was performed in the submodel under the boundaries of the concerned joints, where boundaries in each time step of the global FE analysis were input to the submodel step by step as constraints.⁴⁷ A temperature of 35°C was applied to the nodes of the rivet shank in the first step of the analysis in the

submodel with the time integration shut down, and then the temperature of these nodes was then reduced to 0°C in the subsequent steps. Responses, such as elastic strains, plastic strains, and stresses, were determined in transient analyses.

Figure 12A presents the x-component stress-time histories of floor-beam-to-truss joints (ie, joints L15 to L19), which are extracted from the nodes of the floor-beam-to-truss joints in the global model when the fatigue truck load crosses the bridge. It reveals that the floor-beam-to-truss joints with the diagonal are subjected larger stress range that that with the upright. According to Figure 12A, the joint L17 may be most vulnerable to the fatigue damage due to suffering the largest stress range, which is up to 20.06 MPa. Figure 12B depicted the elastic strain contour of the joint L17 under self-weight. It is observed that strains of the joint are in a low level, indicating that the joint is in elastic stage under self-weight.

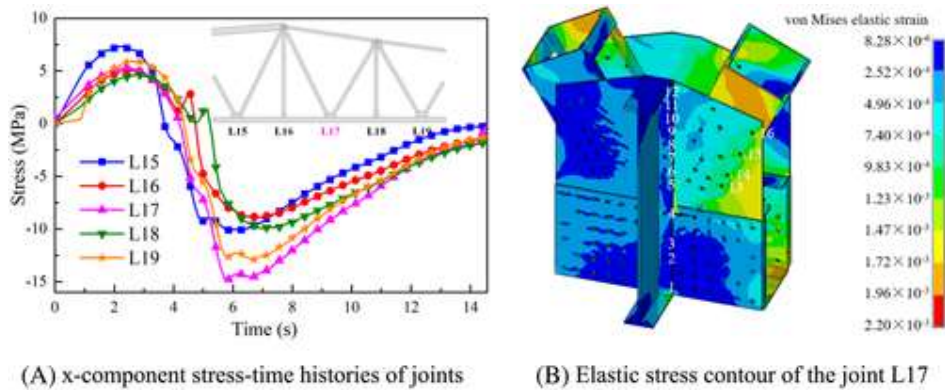


Figure 12

[Open in figure viewerPowerPoint](#)

Stress-time histories of floor-beam-to-truss joints and elastic stress contour of the joint 17 [Colour figure can be viewed at wileyonlinelibrary.com]

To investigate the strain distribution around the rivet hole, strain information of rivet holes labelled as 1 to 16 in Figure 12B is extracted. Figure 13A,B presents the elastic strain time histories of the Hole 1 and 12 in the replaced member (ie, floor-beam), indicating that the rivet holes are subjected to alternative strains. It is observed that the strain responses of difference points of the same hole are similar in pattern; however, significant difference exists in magnitude due to strain concentration. Taking the Hole 12 as an example, Figure 13C shows the circumferential elastic strains of points around its end in time step 3 and 6, indicating that significant strain concentration exists between the region within 30° and 60°. Figure 13D further illustrates the strain contour around the Hole 12 in time step 3 and 6, confirming the strain concentration. Note that the strains around the Hole 1 and 12 are in a low level without plastic deformation.

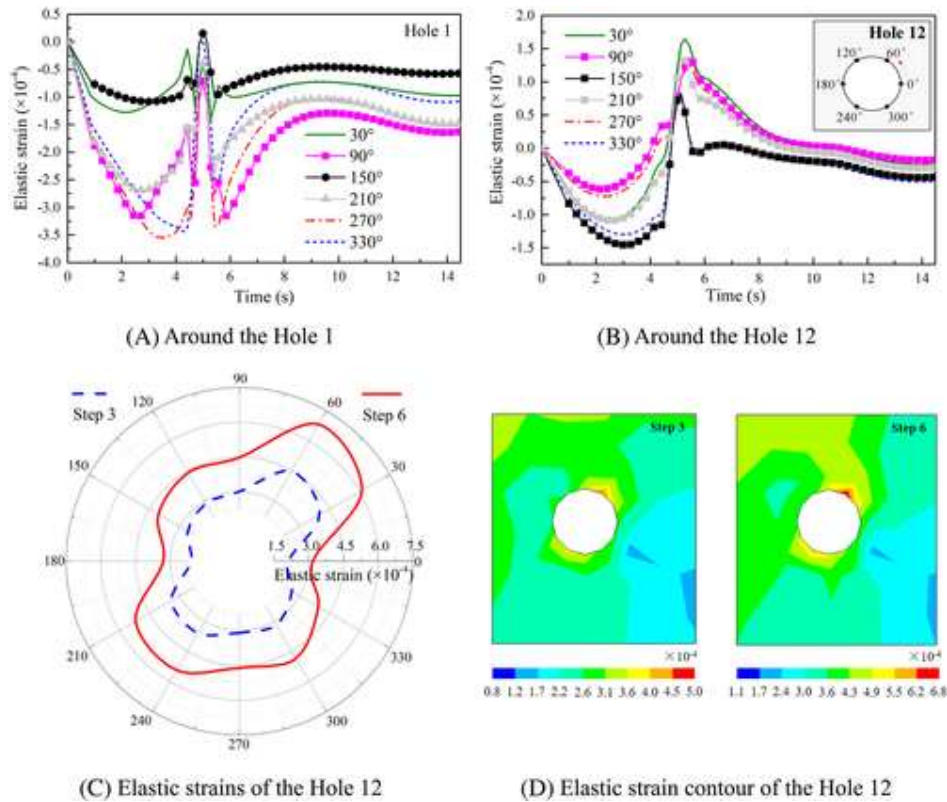


Figure 13
[Open in figure viewerPowerPoint](#)

Elastic strains of points around the Hole 1 and 12 [Colour figure can be viewed at wileyonlinelibrary.com]

Figure 14 presents the elastic and plastic strains of the Hole 15, which is in the original member (ie, gusset plate). The Hole 15 is subjected more significant alternative strains than the Hole 1 and 12 according to Figures 14 and 13. Different from the holes in the floor-beam only subjected to elastic strains, the Hole 15 that is in the gusset plate is subjected to both elastic and plastic strains due to larger load and lower material properties. As shown in Figure 14B, only the regions around the 0° and 180° exist plastic strains, indicating that those regions suffer significant strain concentration and reach the elastoplastic phase. Figure 14C,D, respectively, illustrates the strain and plastic strain contours of the Hole 15, identifying such strain concentration effect. According to Figure 14B,D, the plastic region gradually develops under alternative load due to the moving truck.

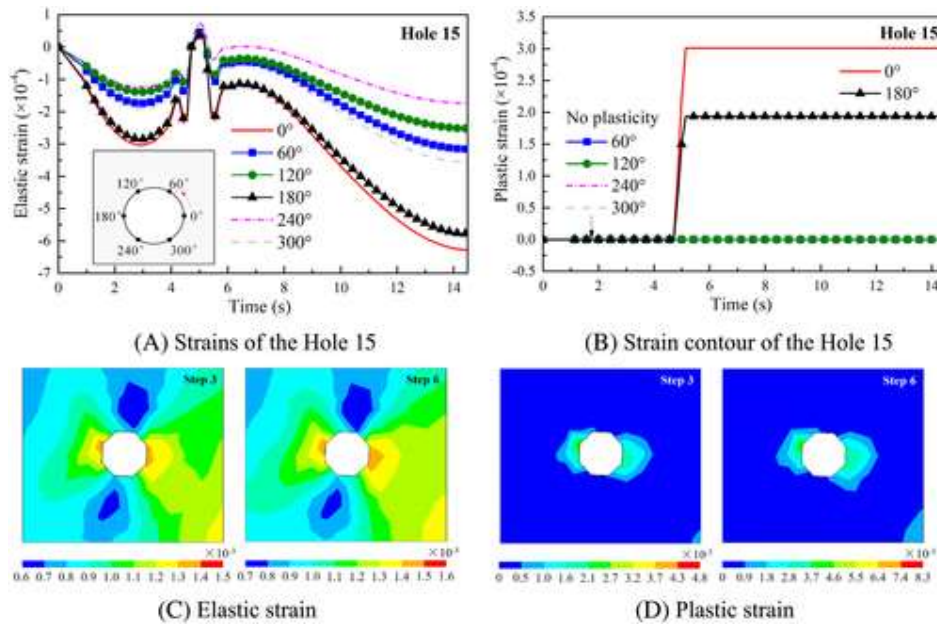


Figure 14
[Open in figure viewerPowerPoint](#)

Elastic and plastic strains of points around the Hole 15 [Colour figure can be viewed at wileyonlinelibrary.com]

3.5 Fatigue life prediction

Strain ranges and number of cycles causing by single truck across the bridge are obtained by using the rain-flow counting. The annual damage index can be derived according to Equation 4 in comprehension with the damage index due to single truck and traffic statistical results, where the average daily volume being 6000 is adopted according to research by Rossigali et al.⁴⁸ Assuming that failure occurs when the cumulative damage exceeds 1, fatigue lives of concerned joint based on the strain states around the rivet holes are determined, as listed in Table 2. The predicted lives of the regions around the riveted hole are longer than 50 years expect for the region around the Hole 15, indicating that in the gusset plate are much more prone to fatigue failure and needs to be strengthened for insufficiency.

Table 2. Fatigue life prediction

Critical Region	$\sum_{i=1}^k \frac{n_i}{N_{f,i}}$	ADTT	Fatigue Life (Year)
Hole 1	8.526×10^{-9}	2.19×10^6	53.6

Critical Region	$\sum_{i=1}^k \frac{n_i}{N_{f,i}}$	<i>ADTT</i>	Fatigue Life (Year)
Hole 12	6.730×10^{-9}		67.8
Hole 13	7.878×10^{-9}		58.0
Hole 15	9.858×10^{-9}		46.3

4 CONCLUSIONS

This study proposed methodology for global-local fatigue analysis and fatigue life prediction is implemented in the riveted joint, incorporating the global structural responses and local plasticity. The procedure for fatigue assessment is demonstrated through a case study of an ancient riveted bridge. According to the research in this paper, conclusions are drawn as follows:

1. Concerned regions of structural members are modelled by using solid elements to capture exquisite detail localized information of fatigue damage, while the large-scale global bridge is primarily created by using beam elements to consider the global fatigue effect. The proposed beam-to-solid submodeling is capable of considering such global structural responses and updating the corresponding variations timely and conveniently, which realizes a good compromise between the simplicity and efficiency for investigating localized nature in depth of large-scale structures. As a result, localized nature (ie, strain concentration), as well as the influence of global structural behavior, can be effectively considered in fatigue assessment.
2. The proposed procedures for global-local fatigue analysis be used to evaluate the fatigue damage of region around the rivet hole effectively, incorporating the global structural responses and local plasticity. Due to the repetitive moving truck loads, floor-to-beam joints are subjected to alternative strains, as well as strain concentration, which can induce significant fatigue damage. Under the continuous loading, the plastic region may gradually develop due to the deterioration of material.
3. Fatigue life can effectively evaluate for the riveted joint according to the proposed methodology. The predicted lives of the regions around the riveted hole are longer than 50 years expect for the region around the Hole 15, indicating that in the gusset plate are much more prone to fatigue failure and need to be strengthened for insufficiency.

